Journal of Molecular Spectroscopy 270 (2011) 123–131

Contents lists available at SciVerse ScienceDirect

Journal of Molecular Spectroscopy

journal homepage: www.elsevier.com/locate/jms

Reexamination of the $C_2H_3^+$ microwave and infrared spectra

Jon T. Hougen [a,*], Laurent H. Coudert [b]

[a] Optical Technology Division, National Institute of Standards and Technology, Gaithersburg, MD 20899-8441, USA
[b] LISA, UMR 7583, CNRS, Universités Paris 12 et Paris 7, 61 Avenue du Général de Gaulle, 94010 Créteil Cedex, France

ARTICLE INFO

Article history:
Received 17 August 2011
In revised form 16 September 2011
Available online 29 September 2011

Keywords:
$C_2H_3^+$
Barrier height
Hydrogen migration
Protonated acetylene
Rotational spectrum
Tunneling splittings
Vibrational spectrum

ABSTRACT

The high-resolution infrared spectrum of $C_2H_3^+$ recorded in the 3μ CH stretching region (J. Phys. Chem. 99 (1995) 15611–15623) is re-analyzed using an effective internal axis method (IAM) Hamiltonian to account for tunneling splittings associated with the large amplitude hydrogen migration motion. The line position analysis carried out with this approach allows us to fit 63% of the data with a standard deviation of 0.05 cm^{-1}, using eight parameters, including the band center, five semi-rigid-rotor spectroscopic constants, and two parameters describing the magnitude of the tunneling splitting and its rotational dependence. The rotational dependence of the observed tunneling splittings is described by an angular offset θ, which can also be calculated theoretically from *ab initio* equilibrium and transition-state structures already in the literature. The agreement between fitted and calculated values of θ, as well as agreement with the value determined from a previous treatment of splittings in the vibrational ground state, gives strong support for the validity of the model. Additional support is provided by the barrier height of 1488 cm^{-1} determined here from the ground state splittings, which agrees well with an *ab initio* estimate of 1300 ± 450 cm^{-1}. The principal problem in the present treatment of the infrared data is the fact that observed minus calculated residuals for 37% of the assigned lines are greater than 0.05 cm^{-1}. This is believed to be due to random perturbations by dark states.

1. Introduction

Although the 3μ infrared spectrum [1,2] and the sub-millimeter-wave spectrum [3,4] of the vibrational ground state of protonated acetylene $C_2H_3^+$ were observed and analyzed some time ago, with help from a variety of theoretical papers [5–10] stimulated by these observations, unanswered questions concerning the hydrogen migration motion in this ion remain. In this paper we revisit the treatment of tunneling splittings associated with this large-amplitude motion (LAM) using an existing high-barrier tunneling Hamiltonian [9,10], in an attempt to evaluate that Hamiltonian's level of success for the ground and one fundamental vibrational state of $C_2H_3^+$, and to suggest new experimental measurements which could increase our knowledge of the $C_2H_3^+$ energy levels and the hydrogen migration motion.

The LAM of interest here is one in which the three H atoms rotate around the C–C core. Pictorial representations of this LAM can be found in Fig. 2 of Ref. [5] and Fig. 1 of Ref. [9], both of which reflect two theoretical assumptions on the hydrogen trajectories, namely that: (i) all five atoms remain in a plane during the LAM, and (ii) the H atoms do not overtake each other. Fig. 3 of Ref. [9] indicates that this LAM can be topologically reduced, for simplicity of classical mechanical, quantum mechanical, and permutation-inversion group theoretical thought, to the internal rotation of an equilateral triangle of H atoms about a stick connecting the two C atoms.

Theoretical discussions in the literature can be divided into two groups. The ground-state sub-mm measurements were first understood qualitatively and explained semi-quantitatively by theoretical works [5–8] based on solving the large-amplitude migration-rotation problem on an *ab initio* potential surface, which turned out to have six equivalent potential minima separated by relatively high potential barriers. In particular, Ref. [6] presents the minimum energy path from the classical to the non-classical configuration, as calculated by several *ab initio* methods, under the assumption that the molecule remains planar along the path. Ref. [7] then uses the CAS SCF path determined in Ref. [6] to predict, without experimental input, the rotational energy levels and internal-rotation tunneling splittings expected in the ground vibrational state.

Solving Schrödinger's equation for motion on a potential surface is certainly the method of choice in principle, but computational limitations often prevent prediction of spectral line positions with residuals comparable to experimental measurement precision. We thus focus here on a phenomenological high-barrier tunneling Hamiltonian method [9–12], summarized briefly in Section 2, which does not require explicit knowledge of the potential energy surface, but which is often capable of spectral fits to experimental accuracy. It should be noted, however, that such a phenomenological

* Corresponding author. Fax: +1 301 975 2950.
E-mail address: jon.hougen@nist.gov (J.T. Hougen).

0022-2852/$ - see front matter © 2011 Elsevier Inc. All rights reserved.
doi:10.1016/j.jms.2011.09.005

Hamiltonian, in contrast to the methods [5–8] described in the preceding paragraph, has no predictive power until its parameters have been determined by a least squares fit of some set of measured and assigned experimental data. Furthermore, the phenomenological Hamiltonian [9–12] used here will only work well for an isolated vibrational state, i.e., a state not suffering from external perturbations.

Although historically the infrared work preceded the sub-millimeter work, we discuss the experimental data in Sections 3 and 4 in the opposite order, to facilitate understanding of the theoretical questions that arise.

2. Brief summary of the high-barrier tunneling formalism

As a simple analogy, consider two ways of treating the rotational levels of a semi-rigid polyatomic molecule: (i) one can diagonalize a matrix containing parameterized matrix elements derived from an effective rotational Hamiltonian with terms of the form $AJ_z^2 + BJ_x^2 + CJ_y^2 - D_J J^4 + \cdots$, or (ii) one can numerically solve Schrödinger's equation for the vibrational and rotational energy levels associated with a calculated *ab initio* potential energy surface. The high-barrier tunneling formalism [11,12] is analogous to (i).

Matrix elements of the one-dimensional tunneling Hamiltonian formalism used here depend on two main parameters. The first parameter involves a relatively familiar concept, since it represents the nearest-neighbor tunneling frequency h in the non-rotating molecule, which corresponds for $C_2H_3^+$ to the frequency of tunneling between an adjacent pair of the six equivalent minima that can be drawn for the approximately T-shaped non-classical equilibrium structure [1,6]. The other parameter is an "angular offset" θ, which is much less familiar and is described in more detail below. This parameter controls (to first order) the J and K variation of the tunneling splittings in the rotating molecule through its appearance in a Wigner $D^J(0,\theta,0)_{KK}$ function, which leads to a damped-oscillation behavior for the tunneling splittings when they are plotted against J for given K.

We stress again that the tunneling model above does not need a potential surface as input and does not return a potential surface as output. All details of the multidimensional potential surface of the molecule that are important for the tunneling motion considered (and its associated tunneling splittings) are replaced in this phenomenological Hamiltonian by the two parameters mentioned above, together with some small J and K centrifugal distortion corrections to these terms.

The appearance of the angular offset θ can be understood relatively easily by spectroscopists familiar with the expression for high-barrier internal-rotation tunneling contributions to energy levels in a near-symmetric top molecule with a methyl top nearly coaxial with the principal rotational a axis (e.g., methanol). As is well known [13], the K-dependence of those tunneling splittings can be represented for A-species levels ($\sigma = 0$) and E-species levels ($\sigma = \pm 1$) by a Fourier series of the form

$$E = F\sum_n a_n \cos[(2\pi n/3)(\rho K - \sigma)], \quad (1)$$

The angle θ in the present formalism is the analog of the quantity $(2\pi/3)\rho$ in the $n = 1$ term of Eq. (1) [14]. This analogy is not perfect, however, since the first term of Eq. (1) gives rise to undamped oscillations in K which are independent of J. Although not discussed in detail here, this imperfect analogy arises mathematically from the fact that hydrogen migration in $C_2H_3^+$ generates angular momentum about the c axis, so that θ appears in the second position in the argument list of the Wigner function $D^J(0,\theta,0)_{KK}$, whereas internal rotation in methanol generates angular momentum about the a axis, so that θ appears in the first position $D^J(\theta,0,0)_{KK}$.

The origin of the angular offset in $C_2H_3^+$, which represents the amount that the whole molecule must be rotated backwards about the c axis to cancel out the angular momentum generated by one step of the hydrogen migration motion, can be described pictorially [9,14] as follows. Let the molecule-fixed axis system for the $C_2H_3^+$ molecule in each of its six minima be chosen with the z axis parallel to the C≡C bond and the y axis perpendicular to the plane of the molecule. The H migration motion then generates, as the molecule moves from one minimum to the next, an angular momentum perpendicular to the molecular plane (i.e., along the c inertial axis) in the molecule-fixed axis system. This angular momentum has a value of $I_{H3} \times 2\pi/6$, where I_{H3} is some average moment of inertia of the H_3 "triangle" [9] during its "rotation" around the C≡C bond. But traditional vibration–rotation theory tells us [15] that large and troublesome first-order energy contributions of Coriolis interactions are removed only in the Eckart axis system, in which there is no residual vibrational angular momentum (to first order). To change to an Eckart system representation in the present case, the angular momentum generated by the H_3 rotation must be canceled by rotating the whole molecule backwards by an angle $\theta = (2\pi/6) \times [I_{H3}/I_{mol}]$, where I_{mol} is the moment of inertia of the whole molecule about its (out-of-plane) $y = c$ axis.

As a result of requiring the molecule to be in an Eckart axis system during its tunneling motion, e.g., as a result of simultaneously rotating the whole molecule backwards in the molecule-fixed axis system during the tunneling motion from minimum 1 to minimum 2, the C≡C bond will no longer be parallel to the z axis when the molecule and its associated rotational wavefunction from minimum 1 reach the position of minimum 2. But when the $1 \rightarrow 2$ tunneling matrix element (or for conceptual simplicity, the $\langle J,K_{a1},K_{c1}|J,K_{a2},K_{c2}\rangle$ overlap integral) is calculated mathematically, all rotational functions must be expressed in the same coordinate system before integrating. Clearly, since the rotational wavefunction from minimum 2 still has its C≡C bond parallel to the z axis, while the rotational wavefunction that "travelled" to minimum 2 from minimum 1 does not, there is some angular offset in the orientation of the two molecule-fixed axis systems. This angular offset is equivalent for the present $C_2H_3^+$ problem to a rotation about the y axis through the angle θ.

For further qualitative understanding, we note that the angular offset θ plays essentially the same mathematical role in this rotational problem as the internuclear distance offset Δr_e plays when calculating diatomic $\langle v'|v''\rangle$ Franck–Condon factors for electronic transitions between two potential curves with different equilibrium bond lengths. We can thus loosely refer to tunneling integrals of the type $\langle J,K_{a1},K_{c1}|J,K_{a2},K_{c2}\rangle$ as rotational Franck–Condon factors. For more information on the mathematical details associated with the rotational offset θ, the reader is referred to Refs. [9,11,12].

3. Ground-state millimeter-wave measurements and fit

Tables 3 and 4 of Ref. [10] show the presently existing 20 submm-wave measurements in the vibrational ground state of $C_2H_3^+$, together with observed-minus-calculated residuals from a least-squares fit to seven S-reduction rotational constants (A, B, C, D_{JK}, D_J, d_1, and d_2) and the two tunneling splitting parameters (h, θ) mentioned above. The fit is excellent, so from one point of view there is nothing more to be done. From another point of view, however, that successful fit cannot be taken as an unequivocal demonstration of the success of the present phenomenological Hamiltonian tunneling formalism for treating H migration motion, because only three observed splittings are fit to two splitting parameters [10].

Even though the present formalism has been successfully applied to a number of other molecules with a variety of LAM

tunneling motions (e.g., to the water dimer with donor–acceptor H-bond interchange and internal rotations of the H_2O moieties [12,16], to the ethylene glycol large amplitude isomerization [17], and to the internal rotation of nitric acid [18]), it is nevertheless desirable to test its applicability to $C_2H_3^+$ more thoroughly, since some of the initial assumptions for the H-migration LAM (e.g., the assumptions that $C_2H_3^+$ remains essentially planar and that one H atom does not overtake another) may in fact not be true. To suggest how one might go about further testing in the ground state of $C_2H_3^+$, we give in Table 1 a slightly expanded and rearranged version of Table 3 of Ref. [10], which contains calculated values for all *b*-type $K_a = 1{-}0$ transitions for the *P*, *Q*, and *R* branches originating in the J_{0J} states with $J \leqslant 11$, as well as the splitting $\Delta\nu(EA)$ between *E* and *A* components of a given asymmetric rotor transition for transitions where both *E* and *A* symmetry species are allowed for the normal isotopolog $^{12}C_2{}^1H_3^+$ by nuclear spin statistics. In addition, for transitions where only the *E* component is allowed, the tunneling shift from the rigid-rotor frequency for this *E* transition, i.e., $\Delta\nu(E) \equiv \nu(E)_{calc} - \nu_{rigid\text{-}rotor}$, is shown.

The experimental evidence for the successful application of the present model to the large-amplitude hydrogen-migration motion in the ground vibrational state of $C_2H_3^+$ can be divided into two types.

Table 1
Calculated frequencies in MHz for the *E* and *A* species μ_b-type $K = 1{-}0$ tunneling-rotational transitions among levels allowed by nuclear spin statistics in the ground state of $^{12}C_2{}^1H_3^+$. Transitions are labeled at the left by $(J_{KaKc})' - (J_{KaKc})''$.

	$\nu_{calc}(E)$[a]	$\nu_{calc}(A)$[a]	$\Delta\nu(EA)$[b]	$\Delta\nu(E)$[c]
P branch				
111–202	234505.785			−0.144
212–303	166076.863[d]	166076.541[d]	+0.322	
313–404	96295.714			−0.061
414–505	25218.714	25218.681	+0.033	
515–606	−47086.046			+0.037
616–707	−120537.740	−120537.512	−0.228	
717–808	−195042.742[e]			+0.103
818–909	−270496.730[f]	−270496.389[f]	−0.341	
919–10010	−346782.792[e]			+0.108
10110–11011	−423775.708[d]	−423775.446[d]	−0.262	
Q branch				
110–101	368572.496[f]	368572.005[f]	+0.491	
211–202	371430.508[e]			−0.144
312–303	375749.474[f]	375749.124[f]	+0.350	
413–404	381565.737[e]			−0.085
514–505	388929.725[d]	388929.572[d]	+0.153	
615–606	397902.544[e]			−0.019
716–707	408557.752[d]	408557.780[d]	−0.028	
817–808	420979.607[e]			+0.030
918–909	435262.446[d]	435262.576[d]	−0.130	
1019–10010	451510.012[e]			+0.047
11110–11011	469832.821[d]	469832.946[d]	−0.125	
R branch				
111–000	431315.551[e]			−0.164
212–101	494034.255	494033.842	+0.413	
313–202	555312.207			−0.099
414–303	615170.752	615170.595	+0.157	
515–404	673642.541			−0.004
616–505	730773.936	730774.061	−0.125	
717–606	786624.128			+0.078
818–707	841264.568	841264.869	−0.301	
919–808	894780.487			+0.108
10110–909	947267.859	947268.158	−0.299	
11111–10010	998835.793			+0.077
12112–11011	1049602.417	1049602.551	−0.134	

[a] From the constants in Table 4 of Ref. [10].
[b] Calculated tunneling splitting between the *E* and *A* species lines in that row.
[c] Calculated tunneling shift of the *E* line from its rigid-rotor position (see text).
[d] Measured as an unresolved blended line and fitted as a blend in Table 3 of Ref. [10].
[e] Measured as a single line and fitted as a single line in Table 3 of Ref. [10].
[f] Measured as a partially resolved line and fitted as two lines in Table 3 of Ref. [10].

First, we note that the *E*–*A* splittings in Table 1 have a maximum magnitude near 500 kHz at low *J*, decrease to nearly zero around $J'' = 5$ or 6, then change sign and increase again in magnitude. The three large splittings indicated by the superscript *d* in Table 1 were obtained by deconvoluting partially resolved doublets in the spectrum and were used in the original fit, as shown in Table 5 of Ref. [10], and agreed well with theory (although as already mentioned, this was essentially a fit of three splittings to two parameters). However, Table 1 also shows that the tunneling shifts of four unblended *E* lines used in the fit [10] range in magnitude from 100 to 160 kHz. The fact that these significantly shifted and precisely measurable unblended *E* lines are also well reproduced by the theory represents a second type of support for the applicability of the model.

Nevertheless, further support would be desirable. First, future instrumental advances (e.g., molecular beam or sub-Doppler measurements) may permit more precise determinations of the splittings and shifts indicated in Table 1. Second, one might look for splittings in transitions involving levels with $K_a \geqslant 2$. The Supplementary Material thus contains predictions for all *b*-type $K_a = 2 - 1$ lines that have $J'' \leqslant 11$ and that fall in the range from 0.4 to 1.9 THz. Note, however, that calculations for these lines involve extrapolation to $K = 2$ rotational levels using constants determined only from $K = 0$ and 1 levels, so that errors of several MHz may occur.

Finally, as a pictorial aid to understanding, Fig. 1 gives a graphical display of somewhat idealized hydrogen-migration tunneling shifts in the ground vibrational state of $C_2H_3^+$ plotted against $J(J+1)$ for $0 \leqslant J \leqslant 9$, in separate *K*-panels for $0 \leqslant K_a \leqslant 3$. This figure is actually an unscaled version of the panels in Fig. 11 of Ref. [9] (to which the reader is referred for a much lengthier discussion), with the $m = 3$ symmetry species changed as appropriate for the now well established [1] non-classical equilibrium configuration, with the $K^{\pm}$ labels related also to $J_{Ka,Kc}$ labels, and with the points for $J = 8$ and 9 added. Tunneling shifts from near-symmetric-top rigid-rotor energies (obtained from the approximate Eqs. (23)–(26) in Ref. [9] rather than from exact matrix-diagonalization calculations [10]) are indicated by solid lines. For a given series of $J_{Ka,J-Ka}$ or $J_{Ka,J-Ka+1}$ levels, i.e., for levels in a given panel, these lines all pass through zero (and change sign) at the same (non-integral) value of *J*. This value of *J* depends on the angular offset θ and is nearly constant for all K_a, except for the two $K_a = 1$ panels, which are strongly affected by asymmetric-rotor-like $\Delta K_a = \pm 2$ tunneling matrix elements. Symbols indicating G_{24} tunneling-rotational symmetry species are placed over all (J,K_a,m) levels allowed by nuclear spin statistics [9] in $^{12}C_2{}^1H_3^+$. These symbols indicate that some $J_{Ka,Kc}$ asymmetric rotor levels have only an *E* species tunneling component, while others have both an E and an A species component. It can be seen from Fig. 1 (and the ground-state *h* parameter in Table 2) that when both *E* and *A* tunneling components are allowed, then the *E*–*A* splitting of a given asymmetric rotor energy level has a maximum unscaled (scaled) magnitude near 3 (250 kHz) at low *J*, which decreases to zero around $J \approx 5.5$, where it changes sign and then increases again in magnitude.

Fig. 1 can also be used to visualize mm-wave transitions between various pairs of allowed tunneling components. The G_{24} electric-dipole selection rules for allowed levels are $A_{2g}^+ \leftrightarrow A_{2g}^-$ and $E_g^+ \leftrightarrow E_g^-$, which corresponds, for the symbols used in Fig. 1, to open circles ↔ filled circles and open squares ↔ filled squares. The *b*-type selection rules appropriate for pure rotational transitions in $C_2H_3^+$ then require that *Q*-branch transitions take the form of lines connecting two levels having the same *J* and appropriately different symmetries in adjacent panels of the upper ($J_{Ka,J-Ka}$) strip or in adjacent panels of the lower ($J_{Ka,J-Ka+1}$) strip. *P* and *R*-branch transitions take the form of lines connecting some level in the $J_{Ka,J-Ka}$ (upper) strip with a level in the $J_{Ka,J-Ka+1}$ (lower) strip having *J* and K_a values that differ by unity from the corresponding upper strip quantum numbers and having an appropriate symmetry.

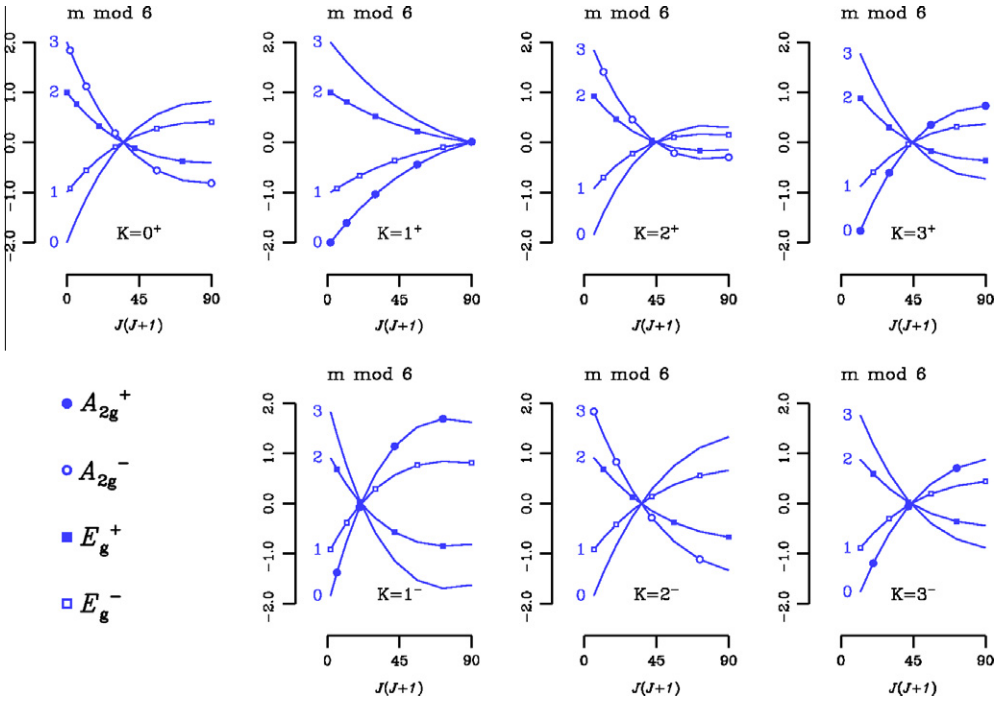

Fig. 1. First-order tunneling splittings (unitless) for levels with $0 \leqslant K_a \leqslant 3$ and $0 \leqslant m \leqslant 3$ in $C_2H_3^+$ (see text) plotted as a function of $J(J+1)$. The top four panels show $J_{Ka,Kc} = J_{Ka,J-Ka}$ states, for $0 \leqslant K_a \leqslant 3$; the bottom three panels show $J_{Ka,Kc} = J_{Ka,J-Ka+1}$ states for $1 \leqslant K_a \leqslant 3$. This figure is essentially a redrawing of the splitting patterns shown in Fig. 11 and Eqs. (23) of Ref. [9], with: (i) symmetry species for the $m = 3$ levels changed to correspond to the non-classical equilibrium configuration [1] of $C_2H_3^+$, (ii) $k_{scale} = -1$ in Eqs. (25) and (26) of Ref. [9], so that the negatives of sums and differences of the Wigner $D^{(J)}\{0,\theta,0\}_{KK'}$ functions [19] are shown, and (iii) $\theta = 0.402665$ rad, as obtained from the fit in Ref. [10]. To obtain the actual first-order tunneling splittings, the ordinate should be multiplied by $|h| = 2.8 \times 10^{-6}$ cm^{-1} (ground state) or $|h| = 0.1115$ cm^{-1} (excited vibrational state) from Table 2. Tunneling splitting contributions are shown for all levels by the solid curves. Levels allowed by nuclear spin statistics for the ground vibrational state of $^{12}C_2H_3^+$ are represented by symbols indicating their torsion-rotation symmetry species, using the notation of Fig. 7 of Ref. [9], i.e., filled and unfilled circles are A_{2g}^+ and A_{2g}^- levels with statistical weight 4, and filled and unfilled squares are E_g^+ and E_g^- levels with statistical weight 2, respectively. Electric-dipole-allowed transitions take place between filled and open circles, or between filled and open squares. Asymmetric-rotor *b*-type *Q* branch transitions correspond to lines connecting appropriate symmetry levels of the same *J* in adjacent *K* panels; *b*-type *P* and *R* branch transitions correspond to lines connecting levels in an upper panel of given *K* with appropriate symmetry and *J* levels in a lower panel labeled by $K \pm 1$. Note that all these *b*-type transitions "go across the tunneling splitting".

Table 2
Fitted values of upper state parameters[a] from a global fit[b] of some[c] of the lines reported in Table 1 of Ref. [2] using the high-barrier tunneling computer program of Ref. [10], together with fitted[d] and calculated[e] values for some of the corresponding ground state parameters.

Parameter[a]	3 μm Value[a]	Gnd. State[d]	*Ab Initio*[e]
ν_0	3142.0867(63)	*f*	
A	13.34975(71)	13.3411020(4)	13.883
B	1.135254(48)	1.1420419(2)	1.144
C	1.040808(38)	1.0464490(4)	1.057
$D_J \times 10^6$	*f*	1.260(2)	
$D_{JK} \times 10^3$	0.1910(52)	0.20141(7)	
$d_1 \times 10^6$	*f*	−0.1116(8)	
$d_2 \times 10^6$	0.712(54)	−0.084(9)	
h	−0.1115(54)	−0.0000028(1)	
θ	0.4046(42)	0.40(3)	0.402

[a] The eight upper-state parameters consist of a vibrational frequency, five of the usual S-reduction rotational and centrifugal distortion constants, a tunneling frequency *h*, and an angular offset θ (see text). All parameters are in cm^{-1} except θ, which is in radians. One standard uncertainty (type A, $k = 1$ [21]) for each parameter is given in parentheses.
[b] The root-mean-square residual for this fit is 0.050 cm^{-1}.
[c] Only 297 of the 468 assigned transitions (63%) in Table 1 of Ref. [2] are included in the fit (see text).
[d] From Table 4 of Ref. [10].
[e] Ground state rotational constants from the MP2/TZ2Pf equilibrium geometry in Table 1 of Ref. [22]. For calculation of the θ value, see the text.
[f] Not used in the fit.

4. 3μ Infrared measurements and fit

Hydrogen-migration tunneling splittings in the infrared spectrum of the fundamental band of the acetylenic asymmetric stretching vibration near 3140 cm^{-1} [1,2] are approximately 30000 times larger than in the ground state (0.3 cm^{-1} vs 0.3 MHz), which, at first glance, makes them very attractive for testing the phenomenological tunneling Hamiltonian under discussion here. Furthermore, an extensive set of assignments in the 3μ infrared spectrum for $0 \leqslant K_a \leqslant 4$ and $0 \leqslant J \leqslant 24$, carried out using ground state combination differences, has been reported [2]. As implied by the discussion in Section 3, ground state rota-

tional levels, at the measurement precision of the infrared spectrum (0.001 cm^{-1}), show no tunneling splittings, which permitted fitting the ground-state microwave measurements truncated to infrared accuracy together with ground-state combination differences from the infrared spectrum to an ordinary asymmetric-rotor Hamiltonian [2]. (We note in passing that ground state rotational levels of $C_2H_3^+$ calculated in this way have recently been added to the Cologne data base for molecular spectroscopy [20].)

After a relatively large number of fits of the assigned transitions reported in Ref. [2] using the program from Ref. [10], we found that the observed-minus-calculated residuals of a relatively unchanging set of strong lines remained in the range of 0.4–1.1 cm^{-1}. This was quite disappointing, because such residuals are significantly larger than the tunneling splittings, which are generally 0.4 cm^{-1} or smaller, and are also hundreds of times larger than measurement error. We considered three plausible explanations for these large residuals: (i) conceptual or programming errors in the present phenomenological Hamiltonian, (ii) assignment errors in Ref. [2], and (iii) perturbations in the 0.5–1 cm^{-1} range of many rotational levels of the upper state of this vibrational band by the numerous unseen and uncharacterized dark states that make up the bath in which this CH stretching fundamental near 3140 cm^{-1} is embedded [8]. We believe, as explained below, that it is random perturbations, rather than program or assignment errors, that are responsible for the fitting difficulties.

4.1. Global fits

Since no global fits of the 3μ spectrum of $C_2H_3^+$ have yet been reported in the literature, we briefly describe our results, focusing on two fits in which we used exactly the assignments and wavenumbers reported in Ref. [2], with two additional remarks. (i) When two alternative assignments were given (indicated by *'d lines in Table 1 of Ref. [2]) we chose for our fit only the alternative that agreed best with our theoretical predictions and discarded the other one. (ii) When the K_c quantum number and/or the A or E symmetry species were not given (mainly for $K_a = 3$, 4, or 5 lines in Table 1 of Ref. [2]), we used the choice for those quantities that gave best agreement with our theoretical predictions.

In one such fit, summarized in Table 2 and deposited in full in the Supplementary Material, 297 $C_2H_3^+$ IR lines are fit to eight parameters with a root-mean-square (rms) residual of 0.050 cm^{-1}. This corresponds (approximately) to using one parameter for every 37 lines, which is not unreasonable. The eight parameters consist of the vibrational frequency v_0, five S-reduction asymmetric-rotor constants (A,B,C,D_{JK} and d_2), and two parameters describing the tunneling splitting (the tunneling frequency h and the angular offset θ (see Section 3)). This set of parameters is also not unreasonable for the $J \leqslant 24$ and $K \leqslant 4$ range of fitted data for this light molecule.

Two characteristics of this fit are quite unreasonable, however. First, only 63% of the 468 assigned lines are included in the fit. Second, the rms of observed-minus-calculated residuals is about 50 times the experimental measurement error, where the latter can be estimated to be 0.001 cm^{-1} either from the halfwidths shown in Fig. 3 of Ref. [2] or from the ground-state combination-difference agreements shown in Table 1 of Ref. [2].

In a second fit (not shown), which was carried out to explore the rms degradation caused by including more measurements, 348 of the 468 lines (74%) were fit to the same 8 constants with a rms deviation of 0.068 cm^{-1} = 68 times measurement error. The nature of the residuals in both of the fits described here is such that adding more adjustable constants to the fit did not significantly reduce the rms.

After carrying out the two fits above, it seemed natural to reexamine the spectral assignments in Ref. [2]. After looking carefully at original spectral records kindly provided by Oka [23], it became evident that a few spectral reassignments could indeed be suggested, but that: (i) such reassignments could reasonably be proposed for only a very small fraction of the "bad" lines, and (ii) they could not reasonably be proposed for any of the strong low-J, low-K "very bad" lines. It thus became unmistakably clear that misassignments in Ref. [2] were not the cause of our 0.5–1 cm^{-1} fitting troubles in the 3μ spectrum of Ref. [2]. To make this discussion more concrete, Table 3 gives illustrations of lines that: (i) fit well, (ii) fit poorly, but could plausibly be reassigned, and (iii) fit poorly, but cannot be reassigned. Even though some improvement in the fit could be expected by a thorough search for reassignment possibilities in the 3μ spectrum, such a search was not carried out here because: (i) it is a very time consuming procedure, (ii) most of the large residuals examined in our preliminary search were associated with clean strong lines, for which no plausible reassignment candidates could be found, and (iii) without double resonance experiments, there is no way to "prove" that any suggested reassignments are actually correct. In short, such a search cannot be expected to lead to significantly stronger experimental support for applicability of the present theoretical model to $C_2H_3^+$.

4.2. J and K dependence of the A–E splittings

One way to organize the tunneling splitting information is to keep K_a constant and list A/E splittings for increasing J, as in Table 4 of Ref. [2]. Symmetry considerations suggest separating even and odd J values, to avoid mixing splittings that involve quite different damped oscillation curves in Fig. 1. Figs. 2–4 thus display observed (thin line with filled circles at each J value) A/E splittings as given in Table 4 of Ref. [2], and calculated (thick line with no points) A/E splittings from the present fit, for the $K_a = 0$, J = even, J_{0J} upper states (Fig. 2), the $K_a = 1$, J = odd, J_{1J} upper states (Fig. 3), and the $K_a = 1$, J = even, J_{1J-1} upper states (Fig. 4). Observed A/E splittings follow the calculated trend moderately well in Figs. 2 and 3, but poorly in Fig. 4.

4.3. Summary of the 3μ fitting situation

Table 2 gives a comparison of the constants obtained from the present fit of tunneling-rotational levels in the asymmetric stretching fundamental state with those obtained from a ground-state fit using the same formalism [10], and with ground-state constants obtained from *ab initio* calculations [22]. It can be seen that fitted values of the rotational constants A, B, C, and D_{JK} in the ground and excited vibrational state are close in value, as would be expected for a small-amplitude vibrational excitation (although the error bars on the excited vibrational state are large because of the poor fit), and that both sets of rotational constants are within 4% of the *ab initio* values. D_J could not be determined in the upper state, presumably because its influence on the high-J energy levels is overwhelmed by the large random perturbations. The tunneling splitting parameter h increases by more than four orders of magnitude upon vibrational excitation, which implies that exciting the acetylenic asymmetric stretch greatly facilitates the H migration. It is thus somewhat surprising, that there is no distortion apparent to the eye of the *ab initio* calculated b_2 (in C_{2v} symmetry) asymmetric C–H stretching harmonic normal mode displacements shown in Fig. 2h of Ref. [24] caused by mixing in some of the calculated b_2 "hydrogen migration internal rotation" harmonic normal mode displacements shown in Fig. 2b, i.e., on the basis of those two figures, one would not intuitively expect such a large increase in the hydrogen migration tunneling frequency upon excitation of the asymmetric C–H stretch. On the other hand, these two vibrations are both of species b_2 in C_{2v}, so it is at least possible to imagine that significant mixing occurs as soon as the large-amplitude

Table 3
Fitting results for representative K_a = 0–0 transitions from Table 1 of Ref. [2].

Assignment[a]		Wavenumber[b]	O–C[b]	Assignment[a]		Wavenumber[b]	O–C[b]
$000A_{2g}^{+}$	$101A_{2g}^{-}$	3140.091	−0.030[c]	$808E_{g}^{+}$	$707E_{g}^{-}$	3158.854	−0.302[g]
$000E_{g}^{+}$	$101E_{g}^{-}$	(3139.787)[d]		$808E_{g}^{+}$	$909E_{g}^{-}$	3121.774	−0.298[g]
				$808E_{g}^{+}$	$707E_{g}^{-}$	3159.188	0.032[h]
$202A_{2g}^{+}$	$101A_{2g}^{-}$	3146.626	0.029[e]	$808E_{g}^{+}$	$909E_{g}^{-}$	3122.104	0.032[h]
$202A_{2g}^{+}$	$303A_{2g}^{-}$	3135.684	0.027[e]				
$202E_{g}^{+}$	$101E_{g}^{-}$	3146.286	−0.053[e]	$10010A_{2g}^{+}$	$909A_{2g}^{-}$	3163.379	0.263[f]
$202E_{g}^{+}$	3 0 3 E_g	3135.346	−0.054[e]	$10010A_{2g}^{+}$	$11011A_{2g}^{-}$	3117.646	0.263[f]
				$10010E_{g}^{+}$	$909E_{g}^{-}$	3163.356	0.095[i]
$404A_{2g}^{+}$	$303A_{2g}^{-}$	3150.912	0.130[f]	$10010E_{g}^{+}$	$11011E_{g}^{-}$	3117.623	0.095[i]
$404A_{2g}^{+}$	$505A_{2g}^{-}$	3131.234	0.131[f]				
$404E_{g}^{+}$	$303E_{g}^{-}$	3150.839	0.166[f]	$16016A_{2g}^{+}$	$15015A_{2g}^{-}$	3175.349	0.086[i]
$404E_{g}^{+}$	$505E_{g}^{-}$	3131.167	0.172[f]	$16016A_{2g}^{+}$	$17017A_{2g}^{-}$	3103.960	0.080[i]
				$16016E_{g}^{+}$	$15015E_{g}^{-}$	3175.398	0.287[f]
$808A_{2g}^{+}$	$707A_{2g}^{-}$	3158.885	−0.123[f]	$16016E_{g}^{+}$	$17017E_{g}^{-}$	3104.016	0.288[f]
$808A_{2g}^{+}$	$909A_{2g}^{-}$	3121.801	−0.123[f]				

[a] Assignments give J_{KaKc} and total vibrational-tunneling-rotational symmetry species for the upper and lower states. Lines are given as *R*-branch/*P*-branch pairs, so that ground-state combination differences can be checked [2].
[b] Observed wavenumbers and observed-calculated (O-C) residuals from the present fit, in cm^{-1}.
[c] Line given in Ref. [1], but not in Ref. [2], since it cannot be confirmed by a P-R branch combination difference check. It was not included in the fit.
[d] Calculated value. No observed candidate available.
[e] Frequencies and assignments from Ref. [2]. These lines fit well and are included in the fit.
[f] Frequencies and assignments from Ref. [2]. These lines fit very poorly and are not included in the fit. No candidates for reassignments could be found in the spectral traces.
[g] Frequencies and assignments from Ref. [2]. These lines fit poorly, and are not included in the fit, but possible alternative assignments exist, as indicated immediately below.
[h] Alternative assignments for the 8 0 8–7 0 7 and 8 0 8–9 0 9 E lines of footnote *g*. These alternatives fit much better, and could be used in a new fit, but without double resonance experiments there is no way to decide experimentally which assignment is actually correct.
[i] Frequencies and assignments from Ref. [2]. These lines fit poorly, but are included in the fit.

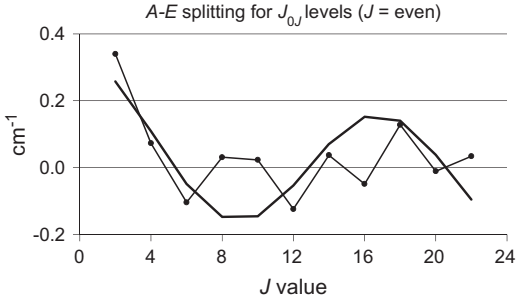

Fig. 2. Observed [2] (filled circles) and calculated (thicker solid line) values for *A*–*E* splittings in the $J_{0,J}$ levels of the C–H asymmetric stretching fundamental state. Because of nuclear spin statistics, this difference can be determined experimentally only for *J* = even. The calculated splittings have a damped-oscillation behavior about zero, that is approximately given (without asymmetric-rotor and centrifugal-distortion effects) by the Wigner function $D^{J}(0,23.18^{\circ},0)_{00}$ [19]. The observed splittings follow this trend, except for *J* = 8, 10, 16, and 22, which represent clear disagreements with the theory. Measurement error is ±0.001 cm^{-1}, i.e., about one tenth the diameter of the filled circles.

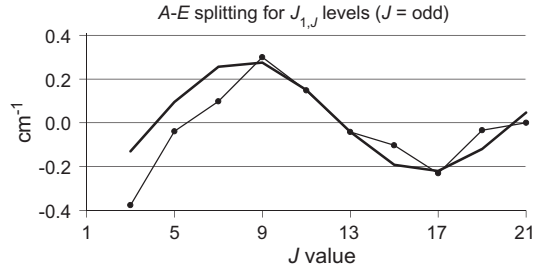

Fig. 3. Observed [2] (filled circles) and calculated (thicker solid line) values for *A*–*E* splittings in the $J_{1,J}$ levels of the C–H asymmetric stretching fundamental state. Because of nuclear spin statistics, this difference can be determined experimentally only for *J* = odd. The calculated splittings have a damped-oscillation behavior about zero, that is approximately given (without asymmetric-rotor and centrifugal-distortion effects) by the difference of two Wigner functions [19] $(1/2)[D^{J}(0,23.18^{\circ},0)_{+1,+1} - D^{J}(0,23.18^{\circ},0)_{+1,-1}]$. The observed splittings (with measurement error ~0.001 cm^{-1}) follow the calculated trend for all *J*.

H-migration tunneling motion progresses far enough to invalidate the small-amplitude harmonic oscillator approximation. (We note in passing that $C_2H_3^{+}$ in its C_{2v} equilibrium configuration has four vibrations of species a_1, one of species a_2, one of b_1 and three of b_2, if the conventions specified in connection with Table III of the Mulliken report [25] are followed, so that the asymmetric C–H stretch at 3140 cm^{-1} should be of species b_2, as in Ref. [24], rather than b_1, as in Ref. [22]. As a consequence of this $b_1 \leftrightarrow b_2$ symmetry species relabeling, the asymmetric C–H stretch should actually be called ν_7, rather than ν_6, as in Refs. [1,2].)

The nearly equal values of the angular offset θ determined from the fits to the ground and excited vibrational state, and from (see Section 5) the *ab initio* structures for the minimum and saddle point [22], give support for the present model, since this parameter is essentially determined by mass and structure considerations (just as the rotational constants are) and would thus be expected to vary between the two fits by about as much as the rotational constants vary (i.e., by less than a few percent), and this is what is observed.

The main conclusion from this section is that the phenomenological tunneling Hamiltonian can describe many, but not all, of the lines in the 3-μm infrared spectrum, but that none of the calculated transitions fit to within experimental error. Our present thinking is that most of the difficulty arises because of extensive perturbations of the CH asymmetric stretching energy levels by surrounding dark states, rather than because of model error, though we have no proof of this.

5. Comparison with *ab initio* results

There are two ways that the fitting parameters from the present treatment can be compared with quantum chemistry results. First,

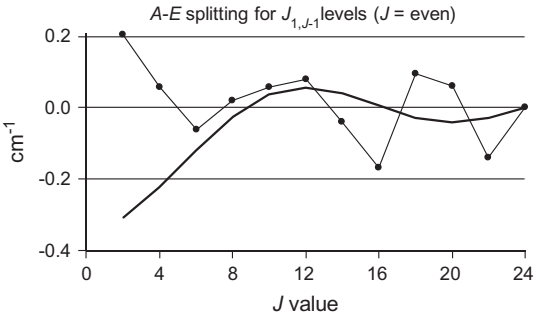

Fig. 4. Observed [2] (filled circles) and calculated (thicker solid line) values for A–E splittings in the $J_{1,\,J-1}$ levels of the C–H asymmetric stretching fundamental state. Because of nuclear spin statistics, this difference can be determined experimentally only for J = even. The calculated splittings have a damped-oscillation behavior about zero, that is approximately given (without asymmetric-rotor and centrifugal-distortion effects) by the Wigner function [19] sum $(1/2)[D^{J}(0,23.18°,0)_{+1,+1} + D^{J}(0,23.18°,0)_{+1,-1}]$. Many of the observed splittings do not agree well with the theoretical curve.

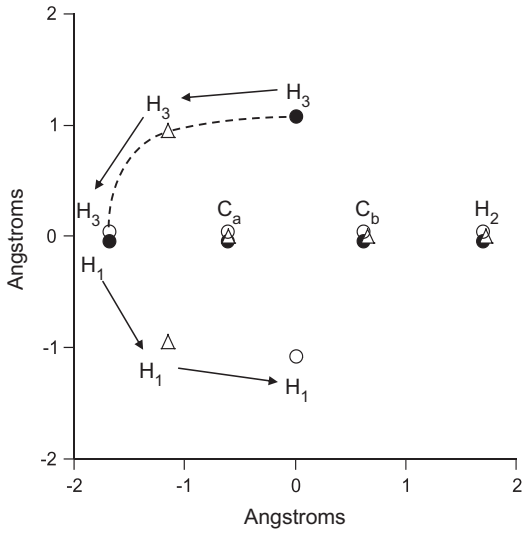

Fig. 5. An overlay of three $C_2H_3^+$ structures from Tables 1 and 2 of Ref. [22], all drawn with their center of mass at the origin and their principal z axes along the abscissa. Solid circles give the equilibrium (nonclassical) structure from Table 1 with H_1–C_a–C_b–H_2 as the nearly linear acetylene moiety and H_3 as the proton attached to the π cloud about 1.12 Å above the z axis. These solid circles can be considered to be the atom starting positions for one step of the hydrogen migration motion. Open circles also give the structure from Table 1, but now with H_3–C_a–C_b–H_2 as the linear acetylene moiety (z axis), and H_1 as the proton attached to the π cloud about 1.12 Å below the z axis. These open circles can be considered to be the atom positions after completion of the first of six steps in a full cycle of the hydrogen migration motion. Open triangles give the saddle-point (classical) structure from Table 2 of Ref. [22], with C_a–C_b–H_2 as the linear part of the vinylidene moiety (z axis), and H_1 and H_3 as the two hydrogens attached to the same carbon atom (C_a). These open triangles can be considered to be the atom positions at the intermediate (saddle) point of the hydrogen migration tunneling path. The • → △ → ○ tunneling trajectory of the H_3 atom is assumed to approximately follow the curved dashed line. A similar pair of arrows has been drawn for H_1, but the dashed curve is omitted to avoid clutter in the diagram. Note that the three atoms C_a, C_b and H_2 barely move during this step of the hydrogen migration.

one can use *ab initio* structural information to estimate a value for the offset angle θ. Second, one can use *ab initio* structural information to estimate an effective moment of inertia for the hydrogen migration motion and then use a conventional internal rotation Hamiltonian to determine a barrier height from the observed tunneling splittings. This "experimental" barrier height can then be compared with *ab initio* values.

In the ideal case, one would want structural information all along the hydrogen migration path, determined by some steepest-descent calculation from the top of the barrier down to the minimum. What is available in the recent literature, however, are quantum chemical structures at two points along the path, one at the non-classical minimum-energy configuration and one at the classical configuration. In particular, Ref. [22] finds that the classical structure corresponds to a first-order saddle point (transition state) at the top of the barrier. Based on the different values given by different computational techniques, they estimate the barrier height to be in the range of $V \cong 1300 \pm 450\ \mathrm{cm}^{-1}$. Ref. [24], on the other hand, gives an estimate of $V \cong 1260\ \mathrm{cm}^{-1}$, with a shallow local minimum slightly below this barrier at the classical configuration. To avoid theoretical complications introduced by this secondary minimum, we use the structures from Ref. [22] in the calculations below.

To visualize one step of the hydrogen migration tunneling path, three structures from Ref. [22] are shown in Fig. 5, all drawn with a common center of mass and a common principal z axis of inertia, as is appropriate when considering the hydrogen migration motion in a molecule in the gas phase. If one assumes that the tunneling motion starts and ends in the non-classical equilibrium structure and passes through an intermediate classical saddle point structure, then the motion of each atom can be approximated by a curved path that starts at a solid circle in Fig. 5, passes through an open triangle, and ends at an open circle. One such a trajectory is indicated schematically by the dashed curve for H_3. Note that only H_3 and H_1 carry out large-amplitude motion during the migration step shown in Fig. 5 (the first of six); the two carbon atoms and the remaining hydrogen barely move.

5.1. The theoretical offset angle θ_{th}

It is relatively straightforward to use the *ab initio* atom positions [22] in Fig. 5, together with five computational simplifications, to obtain a theoretical estimate θ_{th} of the offset angle. The first step involves calculating the angular momentum generated about the center of mass of the molecule by the hydrogen migration motion. Since one of the initial hypotheses of the present model is that all five atoms of $C_2H_3^+$ remain in the xz plane during this large amplitude motion (LAM), the angular momentum generated will always point out of the plane of the molecule. The first four computational simplifications and their intuitive justifications are then as follows. (i) The atom positions for the starting, intermediate, and final configurations in Fig. 5 suggest that it is a good approximation to consider contributions to the angular momentum only from H_1 and H_3. H_2 has the same mass as H_1 and H_3, but it barely moves during the LAM, so its contribution should be negligible. C_a and C_b are much heavier than the H atoms, but their small motions generate contributions to the angular momentum about the center of mass which have similar magnitude, but opposite sign. Their combined contribution should thus involve significant cancelation, and therefore also be negligible. (ii) Instead of calculating the angular momentum generated about the true center of mass of the molecule, we calculate it about the midpoint of the C_a–C_b bond, which lies very close to the center of mass. In addition, the true center of mass moves from one side of the C_a–C_b bond to the other during each of the six steps of the hydrogen migration motion, so that using some "average" position located at the midpoint of this bond is not an unreasonable approximation. (iii) We assume that the initial motion of H_1 in Fig. 5 corresponds to that produced by rotating the C_a–H_1 bond about the C_a atom with an angular velocity $d\alpha/dt$, and that the initial motion of H_3 corresponds to that produced by rotating the C_a–H_3 bond about the C_a atom in the same sense and with the same angular velocity, but shortening the C_a–H_3 bond as it rotates, so that the starting H_3 motion is parallel to the C_a–C_b bond. This corresponds pictorially to imagining that the "track" along

which all hydrogen atoms move resembles an ellipse centered at the midpoint of the C_a–C_b bond, with major axis parallel, and minor axis perpendicular, to this bond. One fourth of this track is indicated schematically by the dashed line in Fig. 5. (iv) We use the MP2/TZ2Pf structures from Tables 1 and 2 of Ref. [22], but change the angle $\angle H_1C_aH_3 = 118.3°$ in Table 1 to $\angle H_1C_aH_3 = 118.7°$, so that the four atoms in the $H_1C_aC_bH_2$ part of the molecule (see the filled circles in Fig. 5) are colinear. Using the atom labels for the black dots in Fig. 5 as subscripts, Table 1 of Ref. [22] then gives $r_{1a} = 1.076$ Å, $r_{3a} = 1.276$ Å, $r_{ab} = 1.224$ Å, and $\angle C_aC_bH_3 \equiv \alpha_0 = 61.3°$. These quantities can be used to define two distances from the center of mass (subscript o), namely $z_{1o} = r_{1a} + r_{ab}/2$ and $x_{3o} = r_{3a}\sin\alpha_0$, which will be useful in the expressions below.

With the assumptions above, the positions and velocities of H_1 and H_3 at the beginning of step 1, as shown in Fig. 5, are

$$\begin{aligned} x_1 &= 0 \qquad & dx_1/dt &= -r_{1a}(d\alpha/dt) \\ z_1 &= -z_{1o} & dz_1/dt &= 0 \\ x_3 &= x_{3o} & dx_3/dt &= 0 \\ z_3 &= 0 & dz_3/dt &= -x_{3o}(d\alpha/dt) \end{aligned} \tag{2}$$

A simple classical mechanical calculation then leads to an angular momentum in the y direction of

$$L_1 + L_3 = m_H(z_{1o}r_{1a} + x_{1o}^2)u\text{Å}^2(d\alpha/dt) \tag{3}$$

at the beginning of the hydrogen migration motion. By symmetry this expression must hold also at the end of the motion, so our fifth computational simplification is to assume that it describes the angular momentum generated all along the hydrogen migration motion.

In the present tunneling formalism, the angular momentum in Eq. (3) must be canceled by rotating the whole molecule backwards about the principal c axis at some smaller angular velocity $-\rho_{\text{th}}(d\alpha/dt)$ [11,12,14], where the dimensionless quantity ρ_{th}, which plays the same role as ρ in the usual internal rotation formalism [13], is chosen to satisfy

$$(L_1 + L_3) - I_c\rho_{\text{th}}(d\alpha/dt) = 0. \tag{4}$$

I_c in Eq. (4) is the value for the moment-of-inertia of the equilibrium structure of the whole molecule about its principal c axis. For the present problem we calculate I_c from the MP2/TZ2Pf structure in Table 1 of Ref. [22], to obtain

$$\rho_{\text{th}} = m_H(z_{1o}r_{1a} + x_{1o}^2)/I_c = 0.1940. \tag{5}$$

This theoretical value for ρ_{th} can then be converted to a theoretical value θ_{th} for the offset angle (the angle of backward rotation of the whole molecule corresponding to one step of the hydrogen migration motion) by using the relation

$$\theta_{\text{th}} = (118.7/120.0)(2\pi/3)\rho_{\text{th}} = 0.402 \text{ radians}, \tag{6}$$

where the $(118.7/120.0)(2\pi/3)$ factor arises because the C_a–H_1 and C_a–H_3 bonds each rotate through an angle of 118.7°. It can be seen from Table 2 that θ_{th} in Eq. (6) is in quite good agreement (to about 1%) with our fitted values for both the ground and excited vibrational states of $C_2H_3^+$.

An estimate of the error bars on θ_{th} can be obtained by calculating ρ_{th} at the saddle-point structure [22], to obtain

$$\rho_{\text{th}}(\text{saddle}) = (L_1 + L_3)/I_c(d\alpha/dt) = 0.1835, \tag{7}$$

which is smaller than the initial ρ_{th} value given in Eq. (5) and used in Eq. (6) by only 6%. If we crudely average the migration path over one third initial part, one third intermediate part, and one third final part, then the value for θ_{th} in Eq. (6) would be decreased by only 2%. The authors consider the results in Eqs. (5)–(7) to be further support for the applicability of the present tunneling model to the hydrogen migration motion in $C_2H_3^+$.

5.2. The "experimental" barrier height V_6

Fits using the phenomenological high-barrier tunneling Hamiltonian suggest that the observed tunneling splittings in $C_2H_3^+$ in the vibrational ground state contain only enough information to determine two independent parameters (h and θ in that model). To determine the barrier height from the tunneling splitting using a more complete one-dimensional LAM model, we need to: (i) choose the LAM coordinate, (ii) set up the kinetic T and potential V energy operators using this coordinate, and (iii) determine the functional form of all molecular parameters in $H = T + V$ along the LAM. Since most of the quantities above are not yet reliably known for $C_2H_3^+$, we resort to use of an approximate Hamiltonian inspired by Fig. 5 and simplified according to the five assumptions of Section 5.1.

At the beginning of the H migration step illustrated in Fig. 5, the non-zero velocities of the atoms of $C_2H_3^+$ in the angular-momentum-free axis system of the backward rotating molecule described in Section 5.1 (which in fact corresponds to the IAM system in traditional internal rotation problems [13], or to the Eckart axis system in traditional vibration–rotation problems [15]) are given by

$$\begin{aligned} dx_1/dt &= -r_{1a}(d\alpha/dt) + z_{1o}\rho_{\text{th}}(d\alpha/dt) \\ dz_3/dt &= -x_{3o}(d\alpha/dt) + x_{3o}\rho_{\text{th}}(d\alpha/dt) \\ dx_a/dt &= -dx_b/dt = +(r_{ab}/2)\rho_{\text{th}}(d\alpha/dt) \\ dx_2/dt &= -z_{1o}\rho_{\text{th}}(d\alpha/dt), \end{aligned} \tag{8}$$

so that the classical kinetic energy expression T at the beginning, and by symmetry at the end, of any given hydrogen migration step becomes

$$\begin{aligned} T &= (1/2)\Sigma_i m_i v_i^2 \\ &= (1/2)m_H(r_{1a} - z_{1o}\rho_{\text{th}})^2(d\alpha/dt)^2 + (1/2)m_H x_{3o}^2(1 \\ &\quad - \rho_{\text{th}})^2(d\alpha/dt)^2 + 2(1/2)m_C(r_{ab}/2)^2\rho_{\text{th}}^2(d\alpha/dt)^2 \\ &\quad + (1/2)m_H z_{1o}^2\rho_{\text{th}}^2(d\alpha/dt)^2 \\ &\equiv (1/2)I_{\alpha,\text{eff}}(d\alpha/dt)^2 = (1/2)(2.5274)u\text{Å}^2(d\alpha/dt)^2. \end{aligned} \tag{9}$$

A subtle point now arises. Because the hydrogen migration motion requires six steps to return the $C_2H_3^+$ molecule to its original atom-numbered configuration, we wish to use a "sixfold-barrier internal rotation Hamiltonian" of the form

$$H = FP_\gamma^2 + (1/2)V_6(1 - \cos 6\gamma) \tag{10}$$

to determine the barrier height V_6 from the observed tunneling splittings. One step of the hydrogen migration motion thus corresponds to a change in γ of 60° in Eq. (10). On the other hand, one step in the hydrogen migration motion corresponds [22] to a change in α of 118.7° in Eq. (9). Making the variable change $\alpha = (118.7/60)\gamma$ in Eq. (9) yields

$$\begin{aligned} T &= (1/2)I_{\alpha,\text{eff}}(d\alpha/dt)^2 = (1/2)I_{\alpha,\text{eff}}(118.7/60)^2(d\gamma/dt)^2 \\ &= (1/2)(9.8917)u\text{Å}^2(d\gamma/dt)^2 \equiv (1/2)I_{\gamma,\text{eff}}(d\gamma/dt)^2, \end{aligned} \tag{11}$$

which then yields a value of $F = 1.7042$ cm^{-1} for use in Eq. (10).

The question of whether Eq. (10) is applicable to the present problem reduces now to the two questions of: (i) whether or not the form of the potential surface along the LAM path resembles a sixfold cosine function, and (ii) whether or not F is approximately constant along that path. The answer to the first question for the potential function shown in Fig. 4 of Ref. [24] is no, since that function has a secondary minimum where the cosine maximum should be. Otherwise, however, the potential curve along the LAM path in

that figure is quite smooth with no unexpected additional structure. The fact that the highest-level calculations of Ref. [22] do not produce a secondary minimum, suggests that high-level calculations will lead to a nearly $\cos 6\gamma$ form for the potential curve along the LAM, and we therefore make that assumption here. The answer to the second question is that the structural parameter F is probably constant to some reasonable approximation, since Eq. (7) shows that the structural parameter $\rho_{\rm th}$ at the saddle differs from $\rho_{\rm th}$ at the minimum by only 6%.

Thus, a calculation using Eq. (10) with $F = 1.7042\ {\rm cm}^{-1}$ from Eq. (11), in which V_6 is adjusted to give agreement with a rotationless ($J = 0$) A–E splitting of $3h = -8.54 \times 10^{-6}\ {\rm cm}^{-1}$ in the ground state [10] gives a barrier height of $V_6 \approx 1488\ {\rm cm}^{-1}$, which agrees well with the *ab initio* estimate of $V_6 \approx 1300 \pm 450\ {\rm cm}^{-1}$ in Ref. [22].

The result of a similar calculation for the excited vibrational state, using $3h = -0.3345\ {\rm cm}^{-1}$ (as given by the fit in Table 2) gives a barrier height of $V_6 \approx 222\ {\rm cm}^{-1}$. This large decrease, which arises because of the increase in observed tunneling splittings by more than four orders of magnitude, suggests (surprisingly) that 40% of the $3142\ {\rm cm}^{-1}$ of C–H stretching vibrational excitation energy can be used to reduce the effective barrier to hydrogen migration.

6. Discussion

In this work we have shown that rotational levels of $C_2H_3^+$ together with their hydrogen-migration tunneling splittings can be treated in a unified way in two different vibrational states, i.e., transitions involving levels in the ground state and in the fundamental of the C–H asymmetric stretch can be fit using the same high-barrier tunneling formalism. The least-squares fits obtained are quite consistent from two points of view. First, nearly the same A, B, C, and D_{JK} rotational constants are found for the two states, and the A, B, C constants agree with recent *ab initio* structures. Second, one of the two parameters in the tunneling part of the formalism, namely an offset angle associated with the amount of angular momentum generated during the large amplitude tunneling motion, is found to be nearly the same for both vibrational states, and the values from these two separate least squares fits agree with a theoretical value calculated from a reasonable tunneling path based on the *ab initio* structural calculations.

Problems with the fit can be seen in the excited vibrational state, however, since: (i) about 1/3 of the assigned levels had to be excluded from the fit because of large observed-minus-calculated values, and (ii) the root-mean-square residual of the fit of the remaining 2/3 of the lines is about 50 times measurement uncertainty. At present, the authors believe that these problems result from many random perturbations in the excited vibrational state, since its position near $3140\ {\rm cm}^{-1}$ means that it is immersed in a relatively dense bath of dark states. The conjecture that the theoretical model is not at fault for these fitting problems could be tested by the acquisition of more experimental data. One possibility is to augment the relatively small sub-millimeter data set in the ground state ($J \leqslant 11$, $K_a \leqslant 1$) by higher J and K measurements (see Supplementary Material for $K_a = 2$ predictions in the THz region). A second possibility is to record and analyze one or more lower lying fundamental transitions in the infrared (see Refs. [22,24] for vibrational frequency and intensity predictions), where perturbations from unknown dark states are expected to cause fewer problems.

In this work we have also shown that the conventional sixfold-barrier internal rotation Hamiltonian for CH_3NO_2 can be used to determine, from the observed tunneling splittings, a barrier to the hydrogen migration motion in the ground state of $C_2H_3^+$ that falls in the range of *ab initio* predictions, provided that structural results from these same *ab initio* calculations for the non-classical equilibrium structure and the classical transition-state structure are used to calculate a realistic value for the coefficient in the kinetic energy operator of this Hamiltonian.

Using the same internal rotation Hamiltonian to treat tunneling splittings in the excited vibrational state leads to a surprisingly large decrease (by nearly a factor of 7) in the effective barrier to hydrogen migration. Here again, study of lower wavenumber vibrational bands in the infrared would tell us whether the excitation of other small-amplitude motions has such a dramatic effect on the hydrogen migration barrier height (or more directly, on the observed tunneling splittings).

Acknowledgment

The authors are deeply indebted to Prof. T. Oka for many discussions, and for making available to them his raw spectral data traces.

Appendix A. Supplementary material

Supplementary data associated with this article can be found, in the online version, at doi:10.1016/j.jms.2011.09.005.

References

[1] M.W. Crofton, M.-F. Jagod, B.D. Rehfuss, T. Oka, J. Chem. Phys. 91 (1989) 5139–5153.
[2] C.M. Gabrys, D. Uy, M.-F. Jagod, T. Oka, T. Amano, J. Phys. Chem. 99 (1995) 15611–15623.
[3] M. Bogey, M. Cordonnier, C. Demuynck, J.L. Destombes, Astrophys. J. 399 (1992) L103–L105.
[4] M. Bogey, H. Bolvin, M. Cordonnier, C. Demuynck, J.L. Destombes, R. Escribano, P.C. Gomez, Can. J. Phys. 72 (1994) 967–970.
[5] R. Escribano, P.R. Bunker, J. Mol. Spectrosc. 122 (1987) 325–340.
[6] R. Lindh, B.O. Roos, W.P. Kraemer, Chem. Phys. Lett. 139 (1987) 407–416.
[7] R. Escribano, P.R. Bunker, P.C. Gomez, Chem. Phys. Lett. 150 (1988) 60–62.
[8] P.C. Gomez, P.R. Bunker, Chem. Phys. Lett. 165 (1990) 351–354.
[9] J.T. Hougen, J. Mol. Spectrosc. 123 (1987) 197–227.
[10] M. Cordonnier, L.H. Coudert, J. Mol. Spectrosc. 178 (1996) 59–65.
[11] J.T. Hougen, J. Mol. Spectrosc. 114 (1985) 395–426.
[12] L.H. Coudert, J.T. Hougen, J. Mol. Spectrosc. 130 (1988) 86–119.
[13] C.C. Lin, J.D. Swalen, Rev. Mod. Phys. 31 (1959) 841–892.
[14] J.T. Hougen, B.M. DeKoven, J. Mol. Spectrosc. 98 (1983) 375–391.
[15] E.B. Wilson Jr., J.C. Decius, P.C. Cross, Molecular Vibrations, McGraw-Hill, 1955.
[16] E. Zwart, J.J. Ter Meulen, W.L. Meerts, L.H. Coudert, J. Mol. Spectrosc. 147 (1991) 27–39.
[17] D. Christen, L.H. Coudert, R.D. Suenram, F.J. Lovas, J. Mol. Spectrosc. 172 (1995) 57–77.
[18] L.H. Coudert, A. Perrin, J. Mol. Spectrosc. 172 (1995) 352–368.
[19] E.P. Wigner, Group Theory, Academic Press, 1959.
[20] H.S.P. Müller, F. Schlöder, J. Stutzki, G. Winnewisser, J Mol. Struct. 742 (2005) 215–227; H.S.P. Müller, S. Thorwirth, D.A. Roth, G. Winnewisser, Astron. Astrophys. 370 (2001) L49–L52; The Cologne Database for Molecular Spectroscopy. <http://www.astro.uni-koeln.de/cdms/>.
[21] B.N. Taylor, C.E. Kuyatt, Guidelines for Evaluating and Expressing the Uncertainty of NIST Measurement Results. <http://www.physics.nist.gov/TN1297>, 2001.
[22] R. Lindh, J.E. Rice, T.J. Lee, J. Chem. Phys. 94 (1991) 8008–8014.
[23] T. Oka, Private communication.
[24] A.R. Sharma, J.-Y. Wu, B.J. Braams, S. Carter, R. Schneider, B. Shepler, J.M. Bowman, J. Chem. Phys. 125 (2006) 224306-1–224306-9.
[25] R.S. Mulliken (unsigned), J. Chem. Phys. 23 (1955) 1997–2011.